Tension behaviour of HNBR and FKM elastomers for a wide range of temperatures

Arne Ilseng[a,b,*], Bjørn H. Skallerud[a], Arild H. Clausen[a]

[a] *Department of Structural Engineering, NTNU, Norwegian University of Science and Technology, 7491 Trondheim, Norway*
[b] *Aker Solutions AS, 3408 Tranby, Norway*

Abstract

This article presents uniaxial tension tests of three different elastomer compounds commonly applied as seal materials in the oil and gas industry. The tests were performed at five different temperatures, ranging from −20 to 150 °C. Optical measurements were used to ensure high quality stress-strain data. The material samples were exposed to a cyclic deformation history, enabling the viscoelastic behaviour to be explored. A considerable effect of temperature changes was found, with a pronounced increase of stiffness and viscosity for the lowest temperatures. A dip in the stress-strain curve was seen for one of the hydrogenated nitrile butadiene rubbers tested at low temperatures. Matrix-particle debonding simulations qualitatively described this stress dip. For the tests performed at the highest temperatures, a considerable number encountered material failure.

Keywords: Elastomers, uniaxial tension, temperature effects, relaxation, failure

1. Introduction

Failure of elastomer seals during qualification testing [1] is an expensive issue for the subsea oil and gas industry. An increased use of numerical calculations, like finite element simulations, during the design of such seals could possibly reduce the number of failed qualification tests and thereby lower costs. To enable predictive results from numerical simulations, constitutive models that capture the essential physics of the material at hand must be employed. The accuracy of the numerical predictions is also strongly dependent on the quality of the experimental tests providing input data to the material model.

Elastomer seals that are used in subsea equipment undergo severe service conditions including high pressures, exposure to production fluids, large deformations, and varying temperatures. In addition to the mechanical features, thermal characteristics like specific heat capacity, thermal conductivity, and thermal expansion are therefore important material properties. The scope of this work is to obtain low strain-rate viscoelastic material data for the large strain behaviour of elastomers at a wide spectre of temperatures, ranging between −20 and 150 °C. Two material

*arne.ilseng@ntnu.no

groups commonly used for sealing purposes in the oil and gas industry; hydrogenated nitrile butadiene rubber (HNBR) and fluoroelastomer (FKM), are addressed herein. HNBR is known as the workhorse in the oil and gas industry due to its good fluid resistance combined with appropriate mechanical properties. FKM compounds are generally more expensive, but inhabit enhanced temperature capabilities for the high temperature regime and an improved compatibility with certain fluids.

Over the years, numerous studies have dealt with different aspects of elastomeric behaviour relevant for sealing application modelling (e.g. [2–10]). However, the number of investigations concerned with the effects of temperature on elastomers mechanical behaviour is limited [11–19]. The general findings though, are that the elastic stiffness and the viscous effects are enhanced as temperature is reduced. A contrary to the latter aspect was shown by Shaw et al. [15] for a natural rubber above its chemorheological temperature, i.e. the temperature above which chain scission is accelerated, where chemical changes ensured a significantly enhanced stress relaxation as the temperature was increased.

For the temperature dependent mechanical behaviour of HNBR and FKM materials specifically, only a few studies could be found in the literature. Rouillard et al. [17] tested an HNBR compound in compression at temperatures between -34 and 80 °C to obtain data for numerical modelling of seals. Khan et al. [18] tested two HNBR compounds in compression at a variety of strain rates and for temperatures ranging from ambient temperature and up to 176 °C. In this temperature range, they found the strain-rate sensitivity to be more pronounced than the temperature effects. For an FKM compound, tension and compression tests at temperatures in the range from -8 to 100 °C were reported by Laurent et al. [19], for the purpose of finite element modelling. They used an optical extensometer to monitor the longitudinal deformation during the tension tests, but only nominal values were reported.

For constitutive modelling of the thermomechanical behaviour of elastomers at large deformations, true stress-strain data obtained by local deformation measurements are of outmost importance. To the best of the authors knowledge, no study presenting such data for HNBR or FKM materials is available in the literature. Nevertheless, Ilseng et al. [9, 10] have recently presented tension and volumetric compression data at room temperature for the HNBR and FKM materials addressed herein. Elastomeric materials are mainly tested in uniaxial tension or compression. In large deformation uniaxial compression tests, frictional forces cause non-homogeneous deformations, making it hard to obtain the correct material behaviour. Tension experiments on the other hand, are far easier to interpret.

The scope of this work is to provide experimental data to be used for constitutive modelling of HNBR and FKM compounds commonly used in sealing applications. True stress-strain data are obtained with local measurements of the deformation field. The study extends the HNBR data available in the literature to cyclic tension, and expands the data for FKM materials to include the

temperature range from −20 to 150 °C. For the high temperature tests, a summary of encountered material failure is presented. In addition, measured values for the heat capacity and thermal conductivity at different temperatures are included for one HNBR and one FKM compound.

The paper is organized as follows: in the subsequent section, the materials and methods used for the experimental work are presented. Next, the obtained experimental results are presented and discussed in Section 3, while some concluding remarks are given in Section 4.

2. Materials and methods

2.1. Materials

Dumbbell shaped specimens of commercially available compounds were ordered from companies supplying seals to the oil and gas industry. All specimens were die stamped from 2 mm thick sheets. One HNBR compound was delivered with a geometry according to ISO 37 type 1 [20], while another HNBR compound and one FKM compound had dimensions in line with ISO 37 type 2. The different materials, their dumbbell geometry, the measured pre-testing density, and the temperature range and hardness values provided by the suppliers are listed in Table 1. The lower end of the temperature range coincides with the temperature at which the material has fully transitioned into the glassy region. The density of the materials was measured both before and after testing; however, no significant density change could be observed. Based on the stated material properties, comparable results would be expected for the two HNBR compounds.

Table 1: Tested materials, their geometries and properties

Material	Geometry	Density	Temperature range	Hardness
HNBR1	ISO 37 - Type 1	1.29 g/cm^3	−35 to 150 °C	86 shore A
HNBR2	ISO 37 - Type 2	1.19 g/cm^3	−29 to 160 °C	89 IRHD
FKM	ISO 37 - Type 2	1.77 g/cm^3	−40 to 200 °C	89 IRHD

2.2. Deformation history

The experimental program was performed using a Zwick/Roell testing machine with a 30 kN load cell and a Zwick WT160 temperature chamber. Liquid nitrogen was connected to the chamber to allow testing below room temperature, while electrical resistance was used for heating. The three materials were tested at five different temperature levels: −20, 0, 23, 85, and 150 °C. Two consecutive tests were run for each combination of material and temperature, giving 30 tests in total.

Since elastomer seals in the subsea oil and gas industry are often exposed to loading cycles, either due to temperature variations, pressure variations, or due to dynamic sealing conditions, a cyclic deformation history was applied. All specimens were exposed to seven loading cycles in total, as illustrated for the HNBR1 material in Figure 1. In each cycle, the sample was stretched

40 mm from its initial length with a deformation rate of 1 mm/s, and unloaded at the same rate of deformation until zero force was obtained in the load cell. Due to the viscous effects in the materials, zero force was measured before the crosshead displacement was back to zero, leading to an effective deformation of less than 40 mm for all cycles but the first one. To get a quantitative measure of the viscous behaviour of the materials, deformation was kept constant at 40 mm for 30 minutes in the sixth cycle as a relaxation test. The maximum displacement was reduced to 30 mm in most high temperature tests, see Section 3.1

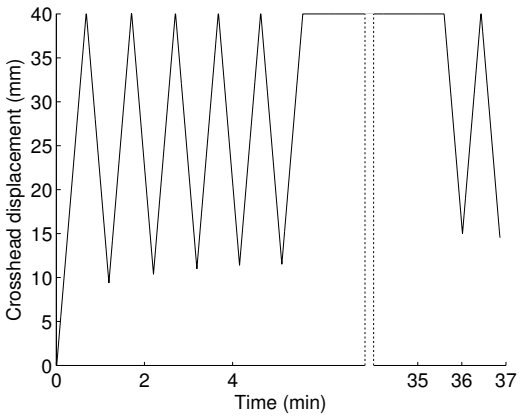

Figure 1: Crosshead displacement for test on HNBR1 at room temperature.

2.3. Determination of true stress-strain curves

The true stress σ obtained in the gauge section of a uniaxial tension test is defined as

$$\sigma = F/A \tag{1}$$

where F is the force applied to the specimen, and A is the current cross-sectional area. The area A can be found from the reference area A_0, being the area measured prior to testing, by the relation

$$A = \lambda_2 \lambda_3 A_0 \tag{2}$$

where λ_2 and λ_3 are the two transverse stretch ratios. When testing at artificial temperatures though, the use of a temperature chamber will often limit the possibility to measure both transverse stretch ratios during deformation. In such a case, an assumption of transverse isotropic material behaviour, i.e. $\lambda_2 = \lambda_3$, can be used to estimate the current cross-sectional area by

$$A = (\lambda_2)^2 A_0 \tag{3}$$

Alternatively, a presumption of material incompressibility can be applied, i.e. the product $\lambda_2\lambda_3$ is uniquely defined from the longitudinal stretch λ_1 through $\lambda_2\lambda_3 = 1/\lambda_1$. This assumption is commonly used for elastomer materials [2], and the current cross-sectional area can be found by the relation

$$A = A_0/\lambda_1 \tag{4}$$

The use of Equation (3) or (4) would significantly simplify the experimental protocol. To investigate how the assumptions of transverse isotropy and constant volume affect the estimate of the true stress-strain behaviour, a separate set of experiments on all three materials was performed at room temperature. In these tests, an Instron 5944 testing machine with a 2 kN load was used. The specimens were exposed to five deformation cycles in which they were loaded to 40 mm of crosshead displacement, and unloaded until zero force was measured by the load cell. A deformation rate of 1 mm/s was applied.

To enable the calculation of local deformations, a random grey scale speckle pattern was spray-painted in the gauge section of the specimens, and two independent cameras were used to capture frames of both the wide and the narrow surface of the samples. The frames obtained during the fifth cycle of the tests were post-processed with an in-house digital image correlation (DIC) software [21] to calculate all three stretch components, and subsequently the true longitudinal strain. The longitudinal stretch calculated from the two independent cameras differed with less than 0.3 %. The deformation in the gauge section of the specimens was also found to be nearly homogenous.

The different stress estimates were compared by calculating the mean stress response, i.e. an average of the loading and unloading curve, for the fifth cycle. A correct true stress-strain response, employing the current area found with Equation (2), was obtained by use of all three measured stretch components. In Figure 2, this correct true stress-strain response is compared with estimates based on information from one camera only. It can be seen that an assumption of constant volume, leading to Equation (4), gives a very good resemblance of the true stress level for both HNBR compounds, with the estimated stress deviating less than 1 % from the correct stress level. For the FKM compound, on the other hand, the estimated peak stress based on a constant volume assumption is more than 18 % above the correct level. Estimating the current area from a transverse isotropy presumption, as defined by Equation (3), the obtained true stress-strain curves are slightly underestimating the correct ones for all three materials.

In the following sections, the constant volume assumption was applied for the two HNBR compounds, while the FKM material was regarded as transverse isotropic. An exception was made for the first loading of HNBR1 at -20 and 0 °C, where the isotropy assumption was used; this is discussed further in Section 3.3.

2.4. Thermal conditioning

Polymeric materials are in general good thermal insulators, implying that it takes some time to heat or cool the entire sample to the desired test temperature. Finite element analyses were used to estimate the time needed to reach a homogeneous temperature throughout the specimens. Such simulations demand knowledge of the thermal properties of the HNBR and FKM compounds. The thermal conductivity and the specific heat capacity of the HNBR2 and the FKM materials were measured by a laser flash method [22]. Four samples of each material were tested at 25, 50, 100, and 150 °C. Measurements at temperatures lower than the ambient level could not be performed

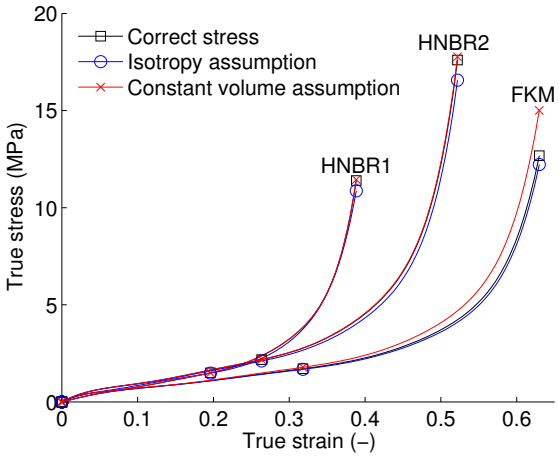

Figure 2: Comparison of true stress-strain curves obtained in three different ways. The mean behaviour of the fifth cycle is shown.

due to limitations in the experimental setup. The results are presented in Figure 3. It appears that the thermal conductivity is rather similar for the two materials, and not very sensitive to temperature. The specific heat capacity differs more, and increases with temperature.

To estimate the coefficient of heat convection between the elastomer compounds and air, a thin rectangular specimen of each material was heated in boiling water, and the temperature decay in room temperature was measured using an infrared thermometer. An air-to-elastomer heat convection parameter of around 15 W/m^{2}K was found for the two HNBR compounds, while a value of 23 W/m^{2}K was determined for the FKM material.

Table 2 shows the conservative thermal data that were used in the numerical simulations to obtain an upper bound estimate of the time needed to heat the specimens. The simulations were carried out using the commercial finite element software Abaqus [23], with a 3D model of the material sample meshed by 1200 elements. The thermal boundary condition was defined as a surface film on the exterior of the specimen. Starting with an initial sample temperature of 23 °C and a chamber temperature of 150 °C, the simulation showed that 15 minutes should be sufficient to heat the samples. For convenience during the experimental campaign, the specimen for test $n+1$ was inserted in the temperature chamber at the start of test n, leading to approximately 40 minutes of thermal conditioning before the specimens were mounted in the test machine.

An important aspect to keep in mind when studying the effect of temperature on inelastic materials is that self-heating might take place during deformation of the samples. By use of an infrared camera, the evolution of temperature during the deformation cycles at room temperature was measured. The peak temperature in the gauge section was found to occur at maximum deformation in the first cycle, with a temperature increase of approximately 4 °C for the HNBR2 material, and about 2 °C for the HNBR1 and the FKM materials. It is presumed that the level of self-heating is somewhat larger at low temperatures, since the plastic work would increase while the specific heat capacity shows a decreasing tendency with reduced temperatures. Nevertheless,

this is considered outside the scope of this work, and the effect of self-heating during deformation is neglected in the further discussion.

Table 2: Material data used for an upper bound estimate of the thermal conditioning.

Thermal conductivity	Specific heat capacity	Density	Air to elastomer convection
0.4 W/mK	2000 J/kgK	1000 kg/m^3	14 W/m^{2}K

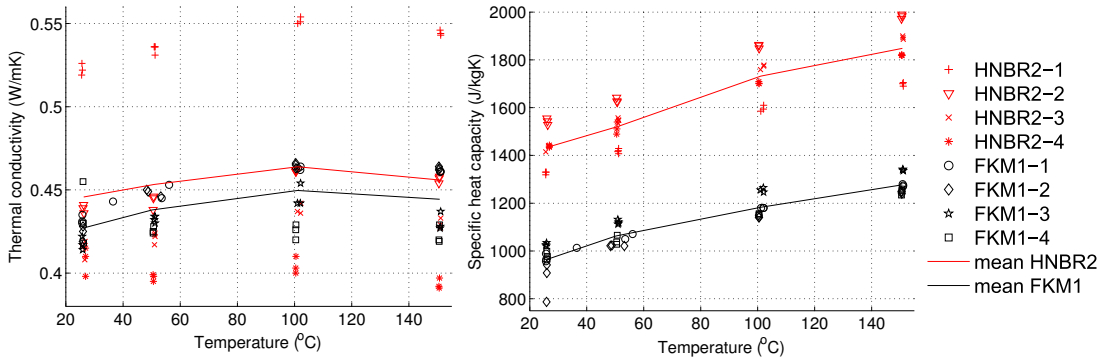

(a) (b)

Figure 3: Thermal properties of HNBR2 and FKM material, measured by a laser flash method (a) thermal conductivity and (b) specific heat capacity.

2.5. Instrumentation

Since there was a single window in the heating chamber, the deformation was measured in the wide surface of the specimens only, using a camera to capture pictures of the gauge section at a frame rate of 7 Hz. To enable optical measurements, a grey scale speckle pattern was spray-painted in the gauge section of the specimens. At low temperatures, cracks formed in the applied paint during deformation, causing difficulties for the DIC software. The pictures of all tests were therefore post-processed by use of an edge trace routine written in MATLAB [24]. In the edge trace routine, the gradient of the grey-scale level in each frame was used to determine both the edge of the specimen and the edge of the painted section. The transverse and longitudinal strains, respectively, were thereafter calculated by looping through all the frames. An example frame from a -20 °C test on an HNBR1 compound is shown in Figure 4a, while the grey level gradient for one vertical line of pixels in the frame is shown in Figure 4b. The edge trace routine was verified at room temperature by comparing the results with those obtained by an in-house DIC software [21]. A difference in the maximum longitudinal strain of less than 0.5 % was found between the two methods.

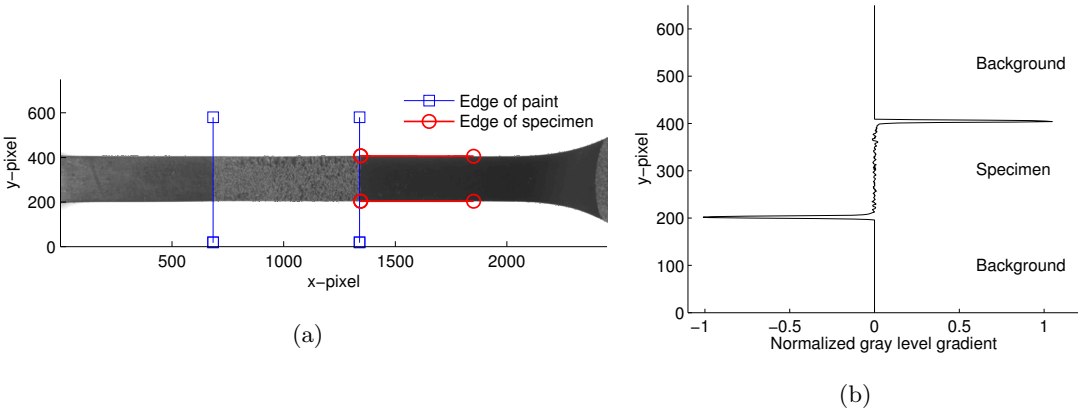

(a) (b)

Figure 4: Example of edge tracing routine for HNBR1 material at −20 °C, (a) example frame and (b) grey level gradient for x-pixel line 1500.

3. Results and discussion

3.1. Preliminaries

In this section, the results obtained from the tension tests at different temperatures are presented and discussed. First, the entire test consisting of seven cycles is addressed in Section 3.2 for all materials and temperatures. Thereafter, a closer look is taken at the first and fifth cycle in Section 3.3 and 3.4, respectively. The sixth cycle, containing the relaxation process, follows in Section 3.5.

Due to material failure at high temperatures, fifth cycle and relaxation results could not be obtained for the FKM compound at 150 °C. In addition, the maximum deformation had to be reduced to 30 mm for the tests on HNBR1 and FKM at 85 °C, and for all materials at 150 °C. All the tests where material failure occurred are presented in Section 3.6.

The curves to be presented in this section were obtained from one of the two tests for each combination of temperature and material. Although not shown herein, the duplicate tests revealed consistency of the presented results.

3.2. Cyclic data

The force-displacement data as obtained from the test machine are presented in Figure 5 for each combination of material and temperature. In general, it can be seen that the main part of the first onloading curve is close to linear, while a more pronounced s-shape can be found in the loading part of the subsequent cycles. The unloading follows a completely different path, especially at low temperatures. The amount of global deformation at the onset of the second cycle is observed to increase significantly as the temperature is reduced. It can be noted that for the HNBR2 material tested at −20 °C, the cycle deformation is less than 10 mm in the fifth cycle, and only a few millimetres in the seventh cycle. In addition to the viscous effects observed through the hysteresis loop, some Mullins softening [25] can be seen for all tests. For the higher temperatures, nearly all

softening happens in the first few cycles, leading to a nearly converged behaviour in the fifth cycle. On the other hand, there is a distinguishable softening occurring also between the fourth and fifth deformation cycle at the lower temperatures. During the first loading of the HNBR1 material at -20 and 0 °C, the force level can be seen to level out and drop slightly after approximately 30 mm of crosshead displacement. This phenomenon is discussed further in the following subsection.

3.3. First loading

Applying the methodology established in Section 2.3, the true stress-strain response for the loading part of the first cycle is shown in Figure 6, where each of the three sub-figures addresses the five temperature levels for one material. The general impression is that the stiffness is reduced as the temperature is increased. In addition, it can be noted that the change of stiffness per degree is lower at elevated temperatures. Comparing the three materials, a pronounced difference in peak stress is observed, especially for the cold temperatures. The HNBR2 has clearly the highest peak stress at -20 °C being nearly 70 MPa, compared to hardly 40 MPa for the FKM material and less than 25 MPa for the HNBR1 material.

During the first loading of the HNBR1 material, a flattening and dip in the stress-strain response was observed for the 0 and -20 °C tests respectively. This low temperature behaviour has already been reported by Rouillard et al. [17], who tested an HNBR compound in uniaxial compression at -34 °C. They suggested that this dip occured due to an elastic-plastic material response. In the present tests however, there is no indication that the HNBR1 material behaves more plastically at low temperatures than the HNBR2 and the FKM compunds, although no stress dip can be seen for those materials. What could be found in the tests, though, was that the rate of transverse deformation, measured on the wide surface of the specimens, dropped to zero at the onset of the stress-dip. This indicates, assuming that the rate of deformation in the thickness direction does not increase correspondingly, that a significant volumetric expansion accompanies the stress-dip. The volume of an elastomer can change in two ways, either by a reconfiguration of the polymer chains, or by an introduction of cavities in the material. The latter, through a matrix-particle debonding process, is expected to be the explanation for the volume increase seen in these tests.

The commercial finite element software Abaqus [23] was used in a generic study of matrix-particle debonding during uniaxial tension. Filler particles in elastomers are known to cluster in grape-shaped structures [8], but for simplicity it was assumed that the global behaviour can be represented by a cylinder of matrix material with a spherical particle embedded in its centre. By use of this simplification, an efficient axisymmetric finite element model could be defined. The model is shown, both in its initial configuration and after debonding has taken place, in Figure 7a. The cell boundaries were constrained to remain straight throughout the deformation, and a Multi Point Constraint user subroutine was defined in Abaqus to ensure a deformation mode of generalized tension. The procedure used was first described by Faleskog et al. [26] for plane strain, and then formulated for axisymmetric models by Kim et al. [27]. Since the HNBR1 material is

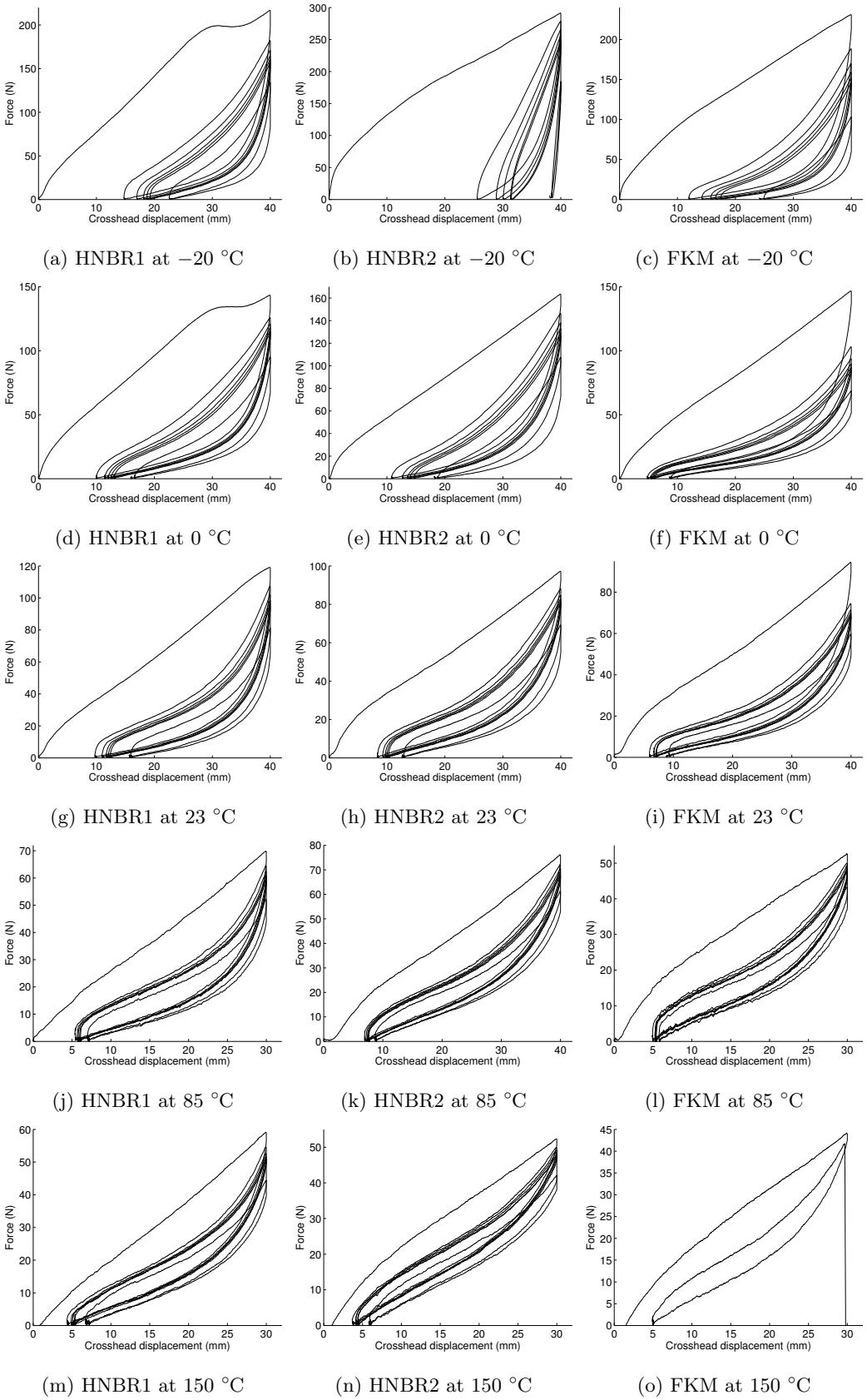

(a) HNBR1 at −20 °C (b) HNBR2 at −20 °C (c) FKM at −20 °C

(d) HNBR1 at 0 °C (e) HNBR2 at 0 °C (f) FKM at 0 °C

(g) HNBR1 at 23 °C (h) HNBR2 at 23 °C (i) FKM at 23 °C

(j) HNBR1 at 85 °C (k) HNBR2 at 85 °C (l) FKM at 85 °C

(m) HNBR1 at 150 °C (n) HNBR2 at 150 °C (o) FKM at 150 °C

Figure 5: Raw machine data for all combinations of material and temperature.

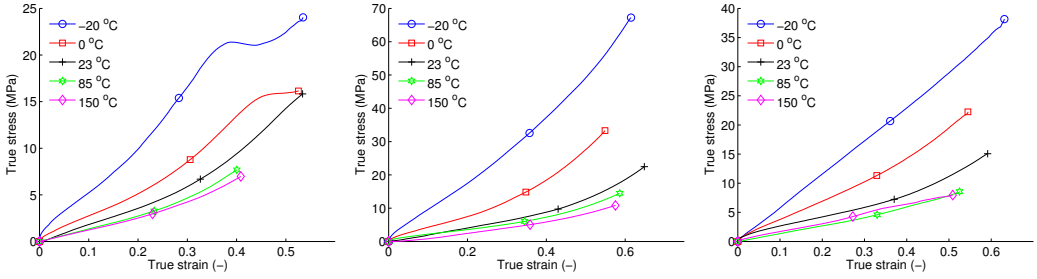

(a) (b) (c)

Figure 6: True stress-strain curves during first loading at different temperatures for the (a) HNBR1, (b) HNBR2, and (c) FKM materials.

a commercial product, the exact amount of filler particles was not known, and the centre sphere was simply assumed to take up 15 percent of the total volume. The matrix material was modelled as an incompressible hyperelastic neo-Hookean material with a shear modulus of 2 MPa, while the filler particle was modelled as linear elastic with a modulus a hundred times larger than the matrix material and a Poissons ratio of 0.3 [8]. Debonding between the matrix and the particle initiated at the pole of the particle, i.e. at the rotation axis, and propagated along the interface towards the symmetry axis of the model. A cohesive zone model was used to define the behaviour of the matrix-particle interface, with the damage initiation and evolution being controlled by a bilinear energy-based criterion.

The stress-strain response obtained from the simulations can be seen in Figure 7b. In addition to one curve representing the approximate qualitative behaviour in the −20 °C test, two curves indicating the effect of increased and reduced fracture energy of the cohesive zone are also included in the figure. A configuration with comparatively low fracture energy, corresponding to the red curve in Figure 7b, is likely to occur at low temperatures. It should be noted that the mechanism shown in Figure 7 might also explain the behaviour observed in compression by Rouillard et al. [17]. In that case, the debonding process would start at the symmetry axis and move towards the rotation axis during deformation.

3.4. Fifth cycle

Since the cyclic behaviour is close to converged after the first four cycles, the fifth cycle can be interpreted as the long-term cyclic behaviour. To obtain comparable data for the different materials, the strain of the fifth cycle was calculated using the configuration at the onset of the cycle as the reference state. An eight-order polynomial was then fit to the stress-strain hysteresis loop to get the mean behaviour of the loading unloading loop. The data obtained for all materials and temperatures are presented in Figure 8. All three materials are seen to exhibit a significantly stiffer behaviour at −20 °C compared to the other temperatures. For HNBR1, little difference can be seen in the cycle behaviour between 0 and 85 °C, while further softening is seen when increasing the temperature to 150 °C. The results for HNBR2 show a clear softening as the temperature is

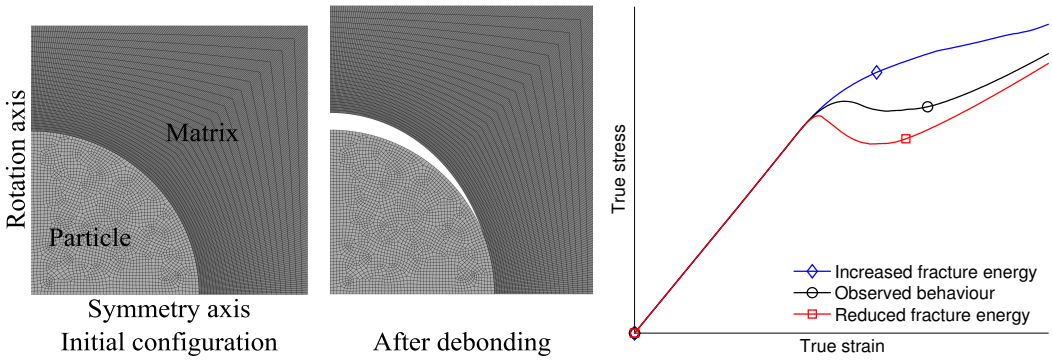

(a) (b)

Figure 7: Finite element results for matrix-particle debonding process. (a) Illustration of the debonding mechanism and (b) the obtained stress-strain data.

increased to 85 °C, but thereafter a slight stiffness increase at large strains for the test performed at 150 °C. In the FKM material, there is little difference between the behaviour at 0 and 23 °C, while the material is slightly stiffer at 85 °C. The 150 °C curve is absent for FKM because these samples fractured during the first or second cycle. The fact that the stiffness of the fifth cycle is increasing at the highest temperatures in the HNBR2 and FKM materials might be due to less cyclic softening occurring during these tests or due to thermal ageing of the materials.

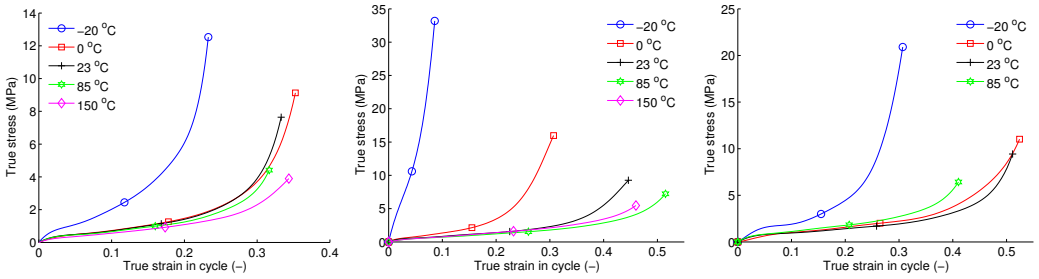

(a) (b) (c)

Figure 8: Fifth cycle mean true stress-strain curve for the (a) HNBR1, (b) HNBR2, and (c) FKM materials.

3.5. Relaxation test

As emphasised in Section 2.2, the specimens were kept at a constant deformation of 40 mm (30 mm for the high temperature tests, see Section 3.1) for 30 minutes during the sixth cycle. The stress relaxation can be defined through a normalized stress $\sigma_N(t) = \sigma(t)/\sigma(t_0)$, where $\sigma(t_0)$ is the stress at the start of the hold period. Figure 9 presents the normalized stress for all materials and temperatures. An exponential decay of the relative stress level with time, as normally found for viscous materials, was observed in all cases. Consistently, the rate of relaxation increased as the temperature was reduced. It is a particular strong relaxation effect at the lowest temperature for the FKM material. These results agree well with the comparatively large hysteresis loops at

low temperatures seen in Figure 5. For temperatures at 0 °C and above, the FKM material has a relative stress level slightly above that of the two HNBR materials, while at a temperature of −20 °C, the FKM material has a significantly lower relative stress. It should be noted that the considerable relaxation occurring in the FKM material at low temperatures would cause a large reduction of the sealing force obtained in a practical application. This could possibly lead to failure of the sealing system due to interfacial leakage.

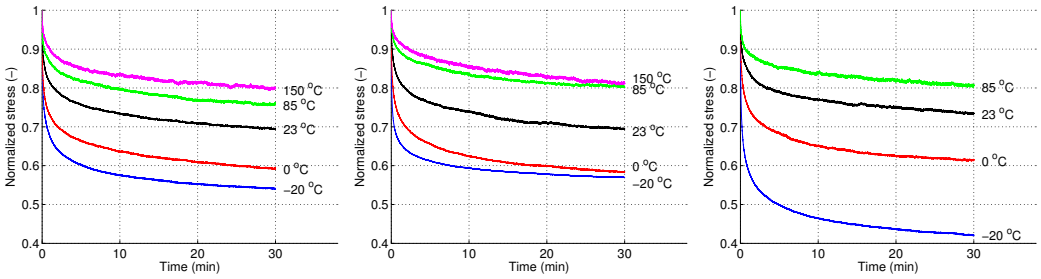

Figure 9: Normalized relaxation behaviour at different temperatures for the (a) HNBR1, (b) HNBR2, and (c) FKM materials.

3.6. Material failure at high temperatures

While no material failure occurred during the tests performed at the three lowest temperatures, this was a considerable challenge for the tests carried out at 85 and 150 °C. Elastomers are in general known to undergo significant chemical degradation, e.g. random chain scission, when exposed to high temperatures [28]. Zhu et al. [29] recently showed that a constant deformation during the high temperature aging process reduced the failure strain significantly for an HNBR compound. It is likely that the chemical degradation caused by the combination of high temperature and large deformation is the reason for the material failures obtained herein.

Table 3 presents an overview of all the tests where material failure was encountered. The table states which material that failed, the test temperature used, if the specimen failed at the clamping or in the gauge section, during which part of the test procedure the failure occurred, at what displacement during a cycle or how long into the relaxation period the failure occurred, and the maximum deformation used in the test procedure. It appears from the table that more than two tests were conducted for the temperatures where failure occurred.

At 85 °C, multiple HNBR1 and FKM samples failed during test series with 40 mm as maximum deformation. Most of these failures occurred by the clamping, and are assumed to be caused by the triaxial stress state that arises in this area. This problem was overcome by reducing the maximum deformation to 30 mm. At 150 °C, one sample of both HNBR compounds failed in the gauge section during the relaxation period, while four consecutive FKM samples failed at this temperature, two by the clamping, and two in the gauge section. FKM compounds are generally

Table 3: Overview of material failure during testing.

Material	Temperature	Failure location	Cycle	Displacement / Time	Max deformation
HNBR1	85 °C	Clamping	Relaxation	3 seconds	40 mm
HNBR1	85 °C	Clamping	First	37 mm	40 mm
HNBR1	85 °C	Clamping	Second	38 mm	40 mm
HNBR1	85 °C	Gauge	Relaxation	8 minutes	40 mm
FKM	85 °C	Clamping	First	33 mm	40 mm
FKM	85 °C	Clamping	Relaxation	23 seconds	40 mm
FKM	85 °C	Clamping	Fourth	36 mm	40 mm
FKM	85 °C	Clamping	Relaxation	13.5 minutes	40 mm
HNBR1	150 °C	Gauge	Relaxation	8.5 minutes	30 mm
HNBR2	150 °C	Gauge	Relaxation	9.5 minutes	30 mm
FKM	150 °C	Gauge	First	25.8 mm	30 mm
FKM	150 °C	Clamping	First	28.3 mm	30 mm
FKM	150 °C	Gauge	Second	29.6 mm	30 mm
FKM	150 °C	Clamping	First	28.3 mm	30 mm

stated to have enhanced high-temperature capabilities compared to HNBR compounds [30]. This capability though, is mainly regarding unstrained aging at high temperatures. When exposed to large tensile deformations combined with the high temperatures however, the results obtained herein indicate that the FKM compound tested is less suited for high-temperature use.

4. Concluding remarks

True stress-strain data was obtained for the cyclic tension behaviour of two HNBR compounds and one FKM compound at a wide range of temperatures. It was shown that HNBR compounds could be assumed to behave incompressible during deformation, while a transverse isotropic assumption had to be used for the FKM compound. In line with previously published results, both elastic stiffness and viscous effects were found to increase as the testing temperature was reduced. In addition, the effect per degree of temperature change was in both cases larger for the lower temperatures.

Comparing the two different HNBR materials, the relaxation behaviour and the elastic response at high temperatures were both found to be comparable. On the other hand, the HNBR2 material revealed a significantly stiffer behaviour than the HNBR1 at low temperatures. In addition, for first loading of the HNBR1 material at 0 and -20 °C, a dip of the stress level could be observed. A considerable volume increase was found to accompany this stress-dip. By use of a finite element model, it was shown that this macroscopic response could be caused by a reduction in the fracture energy for the interface between the matrix material and the filler particles at low temperatures.

Significant material failure was observed for the tests performed at the highest temperatures. For the HNBR1 and the FKM material, the maximum deformation had to be reduced to 30 mm for the tests at 85 °C. At 150 °C, using 30 mm as the maximum deformation, failure in the gauge section was seen for all three materials. For the FKM material, failure occurred during the first few cycles in four consecutive tests, and cyclic material data could not be obtained at this temperature.

In summary, it can be seen that the FKM compound can be challenging as a sealing material at the temperature boundaries. At high temperatures, the material was found to be prone to failure when exposed to tensile loading, while at low temperatures there is a high level of stress relaxation that would lead to a reduced sealing force, and thereby an increased leakage risk. The HNBR materials seem to be less susceptible to failure, and the viscoelastic properties are less sensitive to the temperature variations typically occurring in subsea sealing applications.

Acknowledgements

Aker Solutions are acknowledged for their financial support to this research. The authors would like to express their gratitude to Mr Trond Auestad for his assistance during the experimental work, Mr Lars Edvard Dhli for his guidance on matrix-particle modelling, and to the suppliers who delivered the tests samples for this work free of charge.

References

[1] ISO, 10423:2009 Petroleum and natural gas industries Drilling and production equipment Wellhead and christmas tree equipment, Tech. rep. (2009).

[2] L. R. G. Treloar, The physics of rubber elasticity, Oxford university press, 1975.

[3] J. de Crevoisier, G. Besnard, Y. Merckel, H. Zhang, F. Vion-Loisel, J. Caillard, D. Berghezan, C. Creton, J. Diani, M. Brieu, F. Hild, S. Roux, Volume changes in a filled elastomer studied via digital image correlation, Polymer Testing 31 (2012) 663–670.

[4] G. MacHado, G. Chagnon, D. Favier, Induced anisotropy by the Mullins effect in filled silicone rubber, Mechanics of Materials 50 (2012) 70–80.

[5] H. Bechir, L. Chevalier, M. Chaouche, K. Boufala, Hyperelastic constitutive model for rubber-like materials based on the first Seth strain measures invariant, European Journal of Mechanics, A/Solids 25 (2006) 110–124.

[6] L. A. Wood, G. M. Martin, Compressibility of Natural Rubber at Pressures Below 500 KG/CM2, Rubber Chemistry and Technology 37 (1964) 850–865.

[7] A. G. James, A. Green, Strain energy functions of rubber. II. The characterization of filled vulcanizates, Journal of Applied Polymer Science 19 (1975) 2319–2330.

[8] J. S. Bergström, M. C. Boyce, Mechanical Behavior of Particle Filled Elastomers, Rubber Chemistry and Technology 72 (1999) 633–656.

[9] A. Ilseng, B. H. Skallerud, A. H. Clausen, Volumetric compression of HNBR and FKM elastomers, Constitutive Models for Rubber IX - Proceedings of the 9th European Conference on Constitutive Models for Rubbers, 2015, pp. 235–241.

[10] A. Ilseng, B. H. Skallerud, A. H. Clausen, Case study of elastomer seals using FEM, MekIT'15 - Eighth national conference on Computational Mechanics, CIMNE, Barcelona, 2015, pp. 203–219.

[11] A. D. Drozdov, J. Christiansen, Thermo-viscoplasticity of carbon black-reinforced thermoplastic elastomers, International Journal of Solids and Structures 46 (2009) 2298–2308.

[12] A. Lion, On the large deformation behaviour of reinforced rubber at different temperatures, Journal of the Mechanics and Physics of Solids 45 (1997) 1805–1834.

[13] A. F. M. S. Amin, A. Lion, P. Höfer, Effect of temperature history on the mechanical behaviour of a filler-reinforced NR/BR blend: Literature review and critical experiments, ZAMM Zeitschrift fur Angewandte Mathematik und Mechanik 90 (2010) 347–369.

[14] J. Martinez, A. Boukamel, S. Méo, S. Lejeunes, Statistical approach for a hyper-visco-plastic model for filled rubber: Experimental characterization and numerical modeling, European Journal of Mechanics - A/Solids 30 (2011) 1028–1039.

[15] J. A. Shaw, A. S. Jones, A. S. Wineman, Chemorheological response of elastomers at elevated temperatures: Experiments and simulations, Journal of the Mechanics and Physics of Solids 53 (2005) 2758–2793.

[16] T. Rey, G. Chagnon, J.-B. Le Cam, D. Favier, Influence of the temperature on the mechanical behaviour of filled and unfilled silicone rubbers, Polymer Testing 32 (2013) 492–501.

[17] F. Rouillard, P. Heuillet, B. Omnes, Viscoelastic characterization at low temperature on an HNBR compound for sealing applications, in: Constitutive Models for Rubber VIII - Proceedings of the 8th European Conference on Constitutive Models for Rubbers, ECCMR 2013, 2013, pp. 591–594.

[18] A. S. Khan, M. Baig, S. Hamid, H. Zhang, Thermo-mechanical large deformation responses of Hydrogenated Nitrile Butadiene Rubber (HNBR): Experimental results, International Journal of Solids and Structures 47 (2010) 2653–2659.

[19] H. Laurent, G. Rio, A. Vandenbroucke, N. Aït Hocine, H. L. G. Rio, A. V. N. Aït, Experimental and numerical study on the temperature-dependent behavior of a fluoro-elastomer, Mechanics of Time-Dependent Materials 18 (2014) 721–742.

[20] ISO, 37:2011 Rubber, vulcanized or thermoplastic - Determination of tensile stress-strain properties, Tech. rep. (2011).

[21] E. Fagerholt, T. Børvik, O. Hopperstad, Measuring discontinuous displacement fields in cracked specimens using digital image correlation with mesh adaptation and crack-path optimization, Optics and Lasers in Engineering 51 (2013) 299–310.

[22] ISO, 22007-4:2008, Plastics - Determination of thermal conductivity and thermal diffusivity - Part4: Laser flash method, Tech. rep. (2008).

[23] Abaqus, 6.13-1, Dassault Systèmes, 2013.

[24] MATLAB, version 8.3.0.532 (R2014a), The MathWorks Inc., 2014.

[25] L. Mullins, Softening of rubber by deformation, Rubber chemistry and technology 42 (1969) 339–362.

[26] J. Faleskog, X. Gao, C. Fong Shih, Cell model for nonlinear fracture analysis - I. Micromechanics calibration, International Journal of Fracture 89 (1998) 355–373.

[27] J. Kim, X. Gao, T. S. Srivatsan, Modeling of void growth in ductile solids: effects of stress triaxiality and initial porosity, Engineering Fracture Mechanics 71 (2004) 379–400.

[28] P. Krzysztof, N. James, Thermal Degradation of Polymeric Materials, Rapra Technology, 2005.

[29] Z. Zhu, C. Jiang, Q. Cheng, J. Zhang, S. Guo, Y. Xiong, B. Fu, W. Yang, H. Jiang, Accelerated aging test of hydrogenated nitrile butadiene rubber using the time-temperature-strain superposition principle, RSC Adv. 5 (2015) 90178–90183.

[30] A. Ciesielski, An Introduction to Rubber Technology, Smithers Rapra Technology, 1999.